Graphic abstract

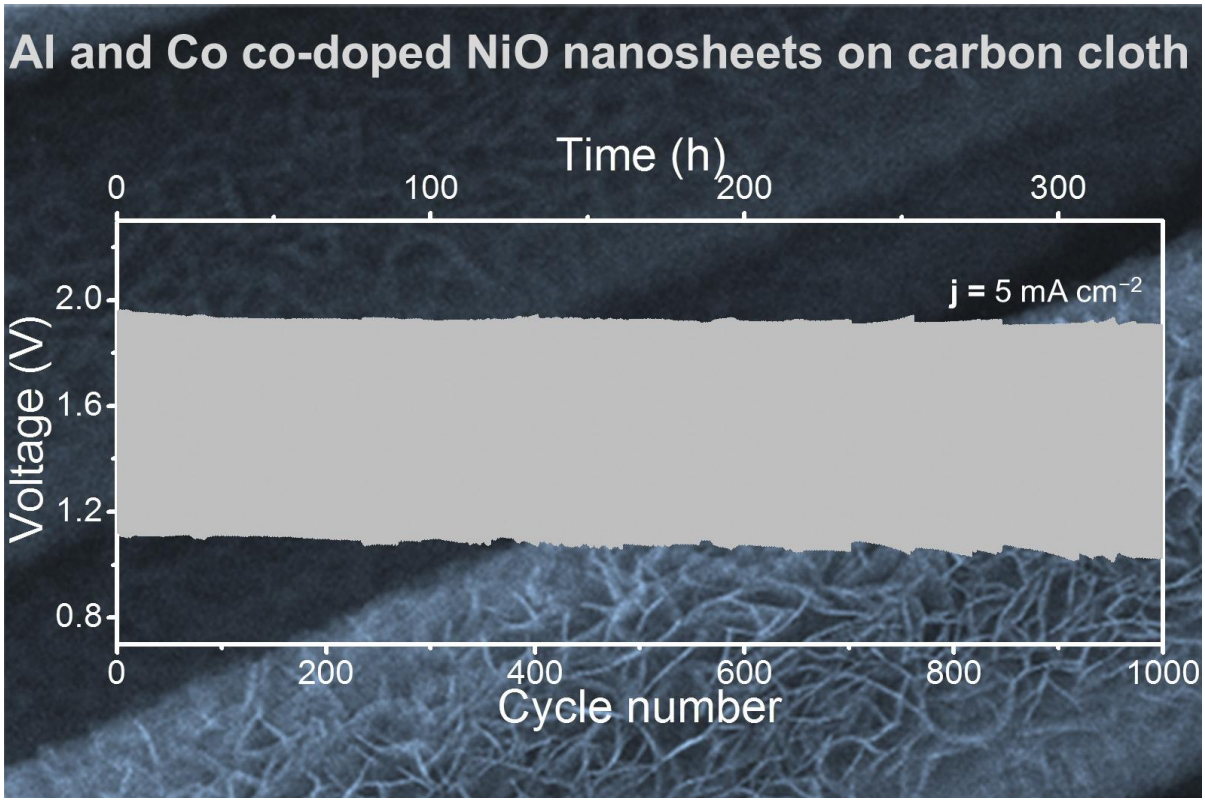

Highlights:

- Al and Co co-doped NiO nanosheets are in-situ grown on carbon cloth.
- Improved activity in both oxygen reduction and evolution reactions is exhibited.
- A Zn-air battery delivers stable voltages and energy efficiency over 1000 cycles.

Growth of Al and Co co-doped NiO nanosheets on carbon cloth as the air electrode for Zn-air batteries with high cycling stability

Peng Tan[1], Bin Chen[1], Haoran Xu[1], Weizi Cai[1], Wei He[1], Meng Ni[1,2,*]

1 Department of Building and Real Estate, The Hong Kong Polytechnic University, Hung Hom, Kowloon, Hong Kong, China

2 Environmental Energy Research Group, Research Institute for Sustainable Urban Development (RISUD), The Hong Kong Polytechnic University, Hung Hom, Kowloon, Hong Kong, China

[*]Corresponding Author, Tel: +852-27664152, E-mail: meng.ni@polyu.edu.hk (Meng Ni)

Abstract: The air electrodes with high activity toward oxygen electrocatalysis and high stability are essential for high-performance Zn-air batteries. Herein, we report an electrode made of Al and Co co-doped NiO nanosheets, which are directly grown on the surfaces of carbon cloth without the addition of binders, facilitating the transport of electrons. Additionally, the hierarchical structure shortens the length for species transport and provides abundant active sites for reactions. In the alkaline solution, the Al and Co co-doped NiO electrode exhibits higher activity in both oxygen reduction and evolution reactions than the pristine NiO electrode without doping and superior stability. When assembled in a Zn-air battery, impressively, this electrode results in stable charge-discharge voltage gaps and energy efficiency of 62% over 1000 cycles (330 h) at 5 mA cm^{-2}. In comparison, a battery with the electrode made of Pt/C and Ir/C shows large voltage gaps and can only be operated for 400 cycles. The characterization of the electrode after cycling illustrates that both the nanosheet morphology and the NiO phase are well maintained. The results demonstrate that the carbon cloth with Al and Co co-doped NiO nanosheets is a promising air electrode to enable the high cycling stability of rechargeable Zn-air batteries.

Keywords: NiO nanosheets; Co-doping; Binder-free; Zn-air battery; Cycling stability

1. Introduction

The increasing demand of electric vehicles and electronic devices requires highly efficient energy conversion/storage systems [1]. To enhance the energy density dramatically, research interest has been devoted to metal-air batteries [2–4]. In particular, Zn-air batteries have become the hot topics due to the high theoretical capacity of zinc (820 mAh g^{-1}) [5]. In addition, oxygen, as the other active component, can be directly got from the ambient air without occupying the mass and volume of the battery, further improving the energy density. Further, the battery is using aqueous electrolytes instead of organic ones, avoiding the safety issue of flammability [6]. The operation of a rechargeable Zn-air battery involves the dissolution and deposition of metallic zinc on the negative (Zn) electrode and the oxygen reduction (ORR) and evolution reactions (OER) on the positive (air) electrode. To make this technology applicable, however, a wide variety of issues should be well solved. In addition to the irreversibility of Zn electrode [7], the sluggish kinetics in the ORR and OER is an obstacle, which not only results in large discharge-charge voltage gaps and low energy efficiency but also the poor cycling stability due to the corrosion occurred at high charge voltages [8]. Therefore, the air electrodes with high activity toward oxygen electrocatalysis and high stability are essential for high-performance Zn-air batteries [9].

Transition metal oxides, due to their high electrochemical performance, low price, and facile synthesis process, have attracted great attention in research [10–13]. Among them, NiO-based materials have been reported as effective catalysts for oxygen electrocatalysis [14–16] and applied in Zn-air batteries [17]. For example, Zong et al. applied Ni/NiO_x nanoparticle-decorated carbon nanofibers in a Zn-air battery and achieved more stable charge voltages in 40 cycles than Pt/C or Ir/C [18]. Guo et al. developed porous NiO/CoN nanowire arrays to promote the electrocatalytic performance and stability. A Zn-air battery with this catalyst exhibited a power density up to 79.6 mW cm^{-2}, an energy density of 945 Wh kg^{-1},

and operating stability for 500 min [19]. Li et al. synthesized Fe_2O_3 and NiO deposited carbon nanotubes, which enabled a Zn-air battery to operate for a continuous cycle of 900 min with a slight degradation of 0.05 V in discharge [20]. Based on the mesoporous spheres assembled by NiO/$Ni(OH)_2$ nanoflakes, Chen et al. developed a hybrid battery combining Zn-Ni and Zn-air reactions, which demonstrated a high power density of 2700 W kg^{-1}, an energy density as high as 980 Wh kg^{-1}, and excellent high-rate charge capability. In our previous work, nanoporous NiO/$Ni(OH)_2$ plates incorporated with carbon nanotubes were developed, which enabled a battery to deliver a high voltage of 1.7 V, a capacity of over 800 mAh g^{-1}, and high cycling stability for over 192 times with maintaining the energy efficiency of over 60% [21]. However, a decrease in the capacity over repeated cycling was observed. This issue in nickel-based materials is caused by the phase conversion of α-$Ni(OH)_2$ in alkaline solutions, which gradually transform to the thermodynamically stable β-$Ni(OH)_2$ [22], decreasing the electrochemical activity and reversibility. To improve the electrochemical performance, introducing other element ions as dopants has been reported as an effective approach [23–25]. Kamath et al. found that nickel-based layered double hydroxides with Cr and Mn can deliver more capacities and more stable in cycling [26]. Li et al. showed that the doping of Co could improve the stability, and at the atomic ratio of 0.57/0.43 for Co/Ni, the sample exhibited 86.4% of the initial capacitance over 1000 cycles [27]. Dai et al. attached the carbon nanotubes with NiAlCo-layered double hydroxide nanoplates, and the results demonstrated that after 2000 charge-discharge cycles, Al and Co co-doping resulted in a slight capacity loss of only ~6% [28].

Herein, inspired by the Al and Co co-doping, we developed an electrode made of Al and Co co-doped NiO nanosheets on carbon cloth for Zn-air batteries in this work. The characterization reveals that porous nanosheets are directly grown on the surface of carbon fibers without the addition of binders, facilitating electron transport. Besides, the hierarchical

structure shortens the length for species transport and provides abundant active sites for reactions. Moreover, Al and Co are successfully incorporated into NiO, which is beneficial for the stability in the long-term discharge-charge cycles. The electrochemical activity of the NiO nanosheets with and without doping was first measured in 0.1 M KOH. Then, a Zn-air battery fitted with the present electrode was assembled, and the discharge and charge performance was tested. Moreover, the cycling stability was evaluated using the pulse discharge-charge method, and compared with the electrode using commercial catalysts (Pt/C and Ir/C). Further, the characterization of the electrode after cycling was carried out to illustrate the morphology and phase changes to demonstrate the stability of the Al and Co co-doped NiO nanosheets electrode.

2. Experimental

2.1 Growth of Al and Co co-doped NiO nanosheets on carbon cloth

The Al and Co co-doped NiO nanosheets on carbon cloth (denoted as NiO-Al-Co/carbon cloth) was fabricated by a modified hydrothermal reaction as previously reported [29]. The carbon cloth was pre-treated through calcination at 500 ^{o}C in air for 4 hours to improve its wettability. Then, the well-cleaned carbon cloth was placed vertically into a Teflon-lined stainless steel autoclave with the capacity of 50 mL. Previous work has demonstrated that Al and Co co-doping with the atomic ratio of 20/2/1 for Ni/Al/Co is effective to stabilize α-$Ni(OH)_2$ [28]. To this end, we chose the same atomic ratio in the fabrication of NiO. Namely, 2 mmol $Ni(NO_3)_2{\cdot}6H_2O$, 0.2 mmol $Al(NO_3)_3{\cdot}9H_2O$, 0.1 mmol $Co(NO_3)_2{\cdot}6H_2O$, 8 mmol $CO(NH_2)_2$, and 4 mmol NH_4F were dissolved in 40 mL of distilled water to form a homogeneous solution. After transferred into the carbon cloth-contained autoclave and sealed, it was maintained at 120 ^{o}C for 7 h in an oven and cooled down naturally to room temperature. The precursor-decorated carbon cloth was taken out, rinsed with distilled water carefully, and dried thoroughly. The calcination process was performed at 350 °C in air for 2

h with a heating rate of 2 ^{o}C min^{-1}. For comparison, the growth of NiO nanosheets on carbon cloth (denoted as NiO/carbon cloth) was fabricated using the similar method without adding $Al(NO_3)_3 \cdot 9H_2O$ and $Co(NO_3)_2 \cdot 6H_2O$. After synthesis, the mass loadings of NiO-Al-Co and NiO nanosheets were measured to be 1.72 and 1.51 mg cm^{-2}, respectively.

2.2 Material characterization

X-ray diffraction (XRD, Rigaku Smartlab) with a Cu-Kα source operating at 45 keV was applied to analyze the compositions of the synthesized samples. The morphologies and nanostructures of NiO-Al-Co and NiO nanosheets decorated carbon cloth were observed by a scanning electron microscope (SEM, VEGA3 TESCAN) under 20 kV and a transmission electron microscope (TEM, JEOL 2100F) with a LaB_6 filament at 200 kV. The elemental concentration and distribution were analyzed on SEM and TEM with energy dispersive X-ray spectrometry (EDS), respectively. The X-ray photoelectron spectroscopy (XPS) data were collected by a Physical Electronics PHI 5600 multi-technique system using Al monochromatic X-ray at a power of 350 W. The adsorption-desorption isotherm was tested on ASAP 2020 Automatic Micropore and Chemisorption Physisorption Analyzer, and the specific surface area and pore distribution were calculated by the Brunaure-Emmert-Teller (BET) and Barrett-Joyner-Halenda (BJH) methods, respectively.

2.3 Electrochemical measurements

A three-electrode cell was applied to measure the electrochemical activity by using the Solartron SI 1287 potentiostat, and the rotation speed was controlled by the instrument from Pine Instrument Co. The working electrode was made by fixing the prepared carbon cloth with NiO-Al-Co or NiO nanosheets on the glassy carbon electrode, the counter and reference electrodes are a platinum wire and a Hg/HgO electrode, respectively, and the electrolyte was 0.1 M KOH. For the ORR test, pure oxygen gas was purged to saturate the electrolyte. Linear sweep voltammetry (LSV) for the ORR polarization was recorded at a scan rate of 5 mV s^{-1}

in the potential range of 0.2 to −0.5 V (vs. Hg/HgO) using the rotation speed from 400 to 2500 rpm. Koutecky-Levich equation was used to determine the number of electrons transferred (*n*):

$$j^{-1} = j_k^{-1} + (0.2nFD_{O_2}^{2/3}v^{-1/6}C_{O_2}\omega^{1/2})^{-1} \quad (1)$$

where *j* and j_k are the measured and kinetic current densities, respectively, *F* is the Faraday constant, D_{O_2} is the diffusion coefficient of O_2 (1.86×10^5 cm^{-2} s^{-1}), v is the kinematic viscosity (1.01×10^{-2} cm^{-2} s^{-1}), C_{O_2} is the bulk concentration of O_2 (1.21×10^{-6} mol cm^{-3}), and ω is the rotation speed (rpm). LSV for the OER polarization was recorded at a scan rate of 5 mV s^{-1} in the potential range of 0.2 to 0.8 V (vs. Hg/HgO) using the rotation speed of 1600 rpm. The ORR and OER stability tests were performed at a constant potential of −0.466 V (vs. Hg/HgO) and a constant current density of 10 mA cm^{-2}, respectively. The cyclic voltammetry (CV) tests were carried out in the potential ranging from 0.2 to 0.7 V (vs. Hg/HgO) using the scan rates from 5 to 40 mV s^{-1}. The specific capacitance value (*C*) was calculated using the following equation [30]:

$$C = \frac{1}{msΔV}\int I(V)\mathrm{d}V \quad (2)$$

where *m* is the mass of NiO-Al-Co nanosheets, *s* is the potential scan rate, ΔV is the potential range, and *I*(*V*) denotes the corresponding current density. The potentials in the following were calibrated to a reversible hydrogen electrode (RHE) scale through:

$$E_{RHE} = E_{Hg/HgO} + 0.059\mathrm{pH} + 0.098 \quad (3)$$

2.4 Fabrication and evaluation of Zn batteries

For the application in Zn-air batteries, the NiO-Al-Co or NiO nanosheets decorated carbon cloth was first soaked in the polytetrafluoroethylene (PTFE) solution with the concentration of 10 wt% and then dried thoroughly [31]. Consequently, a hydrophobic surface was created to facilitate gaseous oxygen diffusion and prevent the leakage of the

liquid electrolyte. A Zn-air battery was assembled using the PTFE-treated sample as the air electrode, which was attached to a gas diffusion layer made of carbon paper. A Zn foil was used as the metal electrode, and 6 M KOH with 0.1 M zinc acetate was applied as the electrolyte. The galvanodynamic voltage profiles of the battery were measured by scaling the current at a step of 1 mA s^{-1}, and the galvanostatic voltage curves were measured at a fixed current density of 5 mA cm^{-2}. The cycling test was performed at 5 mA cm^{-2} for each state of charge (10 min) and discharge (10 min). For comparison, 20% Pt/C and 20% Ir/C were mixed with PTFE based on the mass ratio of 40: 40: 20, and then coated on carbon cloth with the same loading to that of NiO-Al-Co. After dried thoroughly, the carbon cloth electrode with commercial catalysts (denoted as Pt/C+Ir/C) was assembled in a Zn-air battery for the test.

3. Results and discussion

3.1 Characterization of NiO-Al-Co nanosheets

From the XRD patterns in Fig. 1a, in addition to the peak ascribing to the carbon cloth substrate, all other diffraction peaks can be assigned to NiO (JCPDS #47-1049) for both NiO and NiO-Al-Co samples, indicating the high purity of the as-synthesized samples. The SEM images of NiO/carbon cloth are displayed in Figs. 1b and S1a, from which the nanosheets with the thickness of 2.5 μm are grown perpendicularly on the surface of carbon fibers and interconnected with each other [29]. For the NiO-Al-Co/carbon cloth, similarly, the nanosheets are perpendicularly covered the carbon fibers and intertwined to form a well-connected network (Figs. 1c and 1d). However, compared with the pristine NiO nanosheets, the interconnected structure becomes loose, and the thickness is reduced to be 2.3 μm (Fig. 1b). The changes in the morphology are thought to be caused by the element doping, since previous research has indicated that the Al doping can affect the growth of α-$Ni(OH)_2$ and lead to smaller nanoplate sizes [32]. The decreased thickness shortens the electron transport

route, and the loose porous structure with large void volume is beneficial for the saturation of electrolyte with the electrode [33]. From the EDS analysis in Fig. 1e, the elements of Ni, Al, Co could be detected, and the atomic ratio of Ni: Al: Co was determined to be 88.2: 9.3: 2.5, close to our design (86.9: 8.7: 4.4).

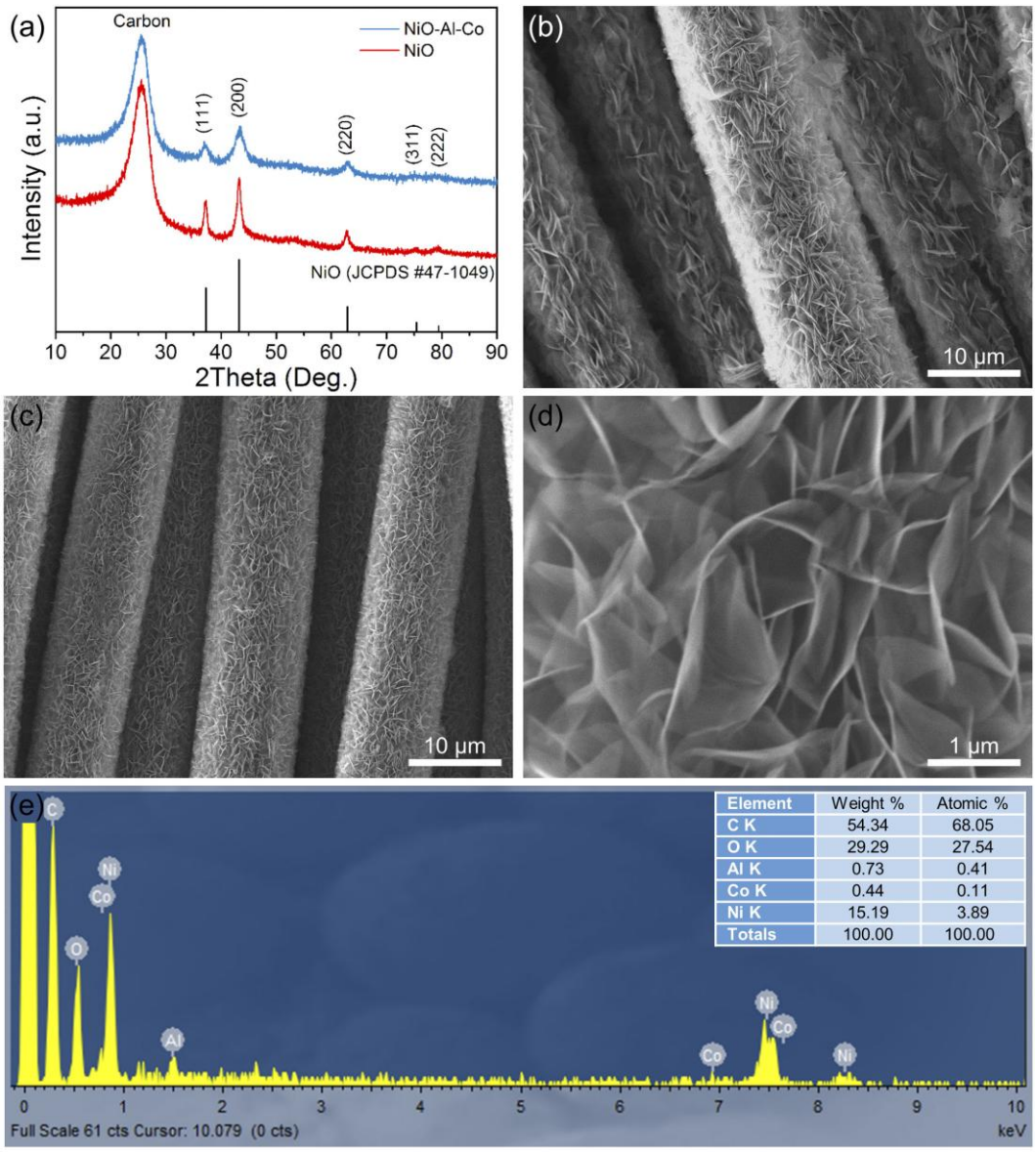

Fig. 1 Characterization of the as-prepared NiO and NiO-Al-Co nanosheets decorated carbon cloth. (a) XRD patterns. (b) SEM images of NiO nanosheets. (c-d) NiO-Al-Co nanosheets at (c) low and (d) high magnifications. (e) EDS analyses, and the inset shows the weight and atomic percentages of detected elements.

The feature of NiO-Al-Co nanosheets is further revealed through TEM analysis, as shown in Fig. 2. Fig. 2a presents the TEM image of one NiO nanosheet, from which the ultrathin nature is clearly demonstrated, consistent with SEM observations. Fig. 2b shows the corresponding high-resolution TEM image, and the lattice spacing of 0.15 nm corresponds to the (220) plane of the cubic NiO phase, confirming the well-crystalline structure. The selected area electron diffraction (SAED) pattern clearly demonstrates the diffraction rings corresponding to the (111) and (220) planes of NiO, indicating the polycrystalline nature of NiO-Al-Co nanosheets. The EDS mapping of Ni, Al, Co, and O shown in Fig. 2c further illustrates that the distribution of Ni, Al, and Co is uniform, corroborating the successful doping of Al and Co into NiO. In addition, the pores distributed uniformly on the nanosheet can be witnessed from Figs. 2a and 2c, which are formed due to the release of water molecules and the shrinkage of the volume of the hydroxide precursor during calcination [34]. Through the nitrogen adsorption-desorption analysis, the NiO-Al-Co/carbon cloth has a specific surface area of 61.33 $cm^2\ g^{-1}$, and most of the pores are in the sizes from 1.8 to 8.6 nm with the average size of 3.4 nm (Fig. S2). This mesoporous structure is important to facilitate the species transport and improve the electrochemical performance [11].

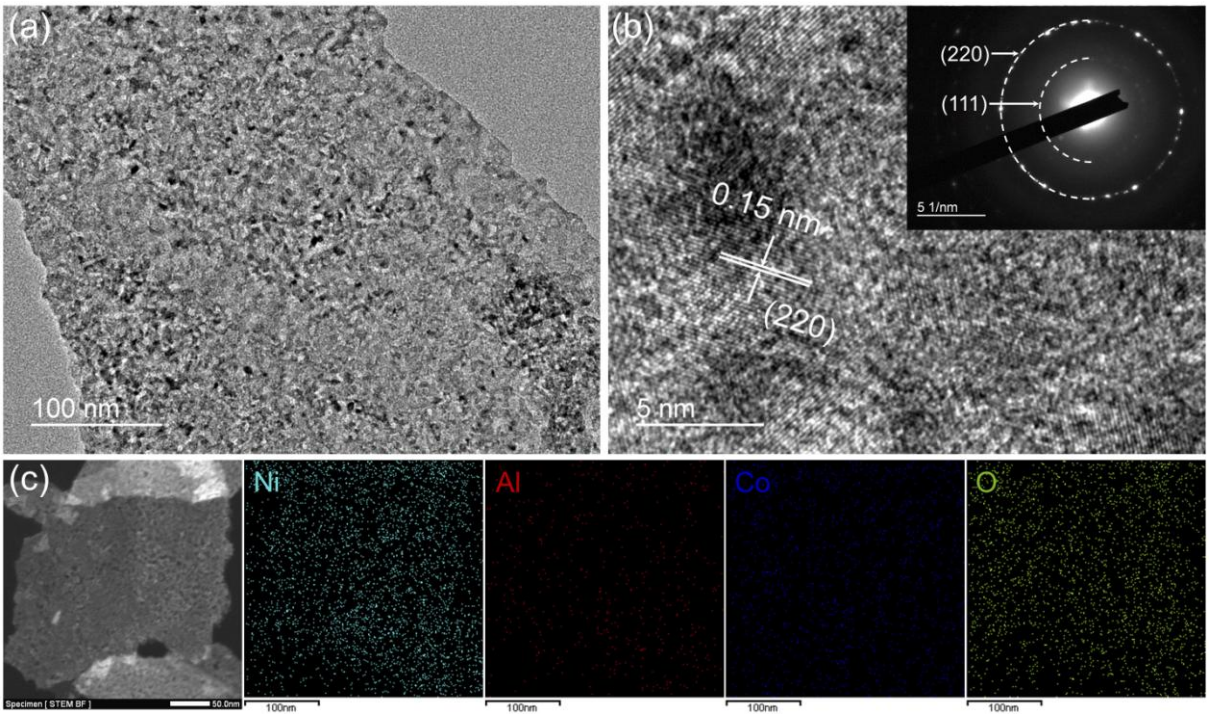

Fig. 2 (a) TEM image of one NiO-Al-Co nanosheet. (b) High-magnification TEM image of the NiO-Al-Co nanosheet. The inset shows the SAED pattern. (c) Simultaneously acquired image and the EDS spectrum imaging for chemical maps of Ni, Al, Co, and O.

The surface electronic states of NiO-Al-Co nanosheets/carbon cloth were further analyzed by XPS (Fig. 3). Fig. 3a is the survey spectrum, from which the presence of C, Ni, Co, Al, and O without other impurities are indicated. The high-resolution Ni 2p spectrum is shown in Fig. 3b, which consists of two spin-orbit doublets. The peaks located at 871.9 eV and 854.2 eV are attributable to Ni^{2+}, and the peaks at 873.1 eV and 856.1 eV are assigned to Ni^{3+}, suggesting the coexistence of Ni^{2+} and Ni^{3+} [35]. Fig. 3c shows the high-resolution Al 2p spectrum, in which one peak with the binding energy of 73.4 eV demonstrates the presence of Al^{3+} [36]. The high-resolution Co 2p spectrum in Fig. 3d is fitted with two spin-orbit doublets, which consists of two spin-orbit doublets at 780.3 eV and 795.0 eV, demonstrating the presence of Co^{2+} and Co^{3+} [37]. The high-resolution O 1s spectrum in Fig. 3e displays the peaks at 529.6 and 531.4 eV that correspond to the oxygen species [38]. From

the XPS analyses, the atomic percentage of Ni, Al, and Co is estimated to be 88.02: 8.90: 3.08, which is consistent with the EDS results.

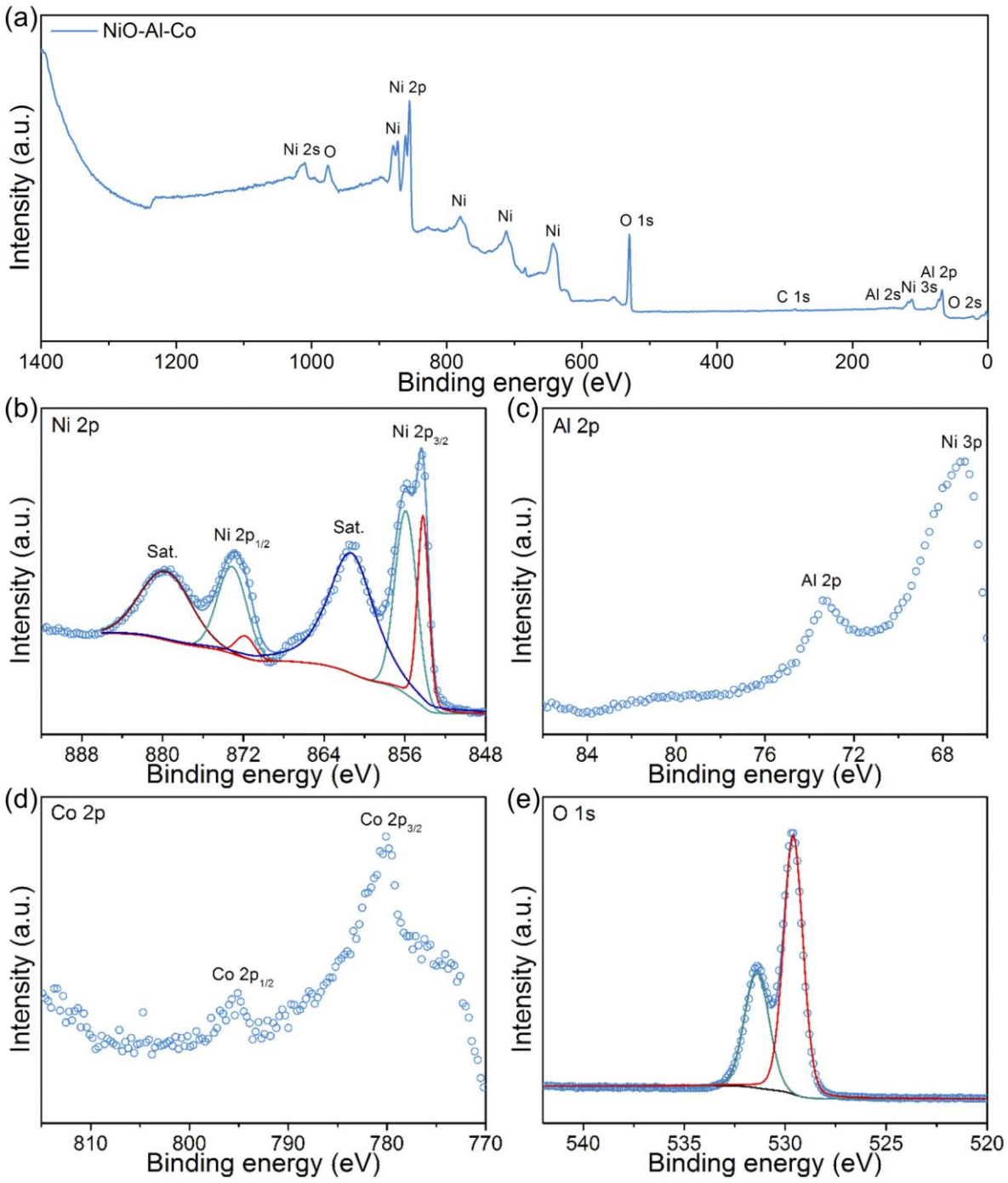

Fig. 3 XPS spectra of NiO-Al-Co/carbon cloth. (a) Survey spectrum. (b-e) high-resolution spectrum of (b) Ni 2p, (c) Al 2p, (d) Co 2p, and (e) O 1s.

3.2 Electrochemical properties

The electrochemical activity of NiO and NiO-Al-Co nanosheets decorated carbon cloth was evaluated in the electrolyte of 0.1 M KOH. In the ORR region, the NiO/carbon cloth exhibited a limiting current density of −4.47 mA cm^{-2} at 0.4 V (vs. RHE) with a Tafel slope of 303.1 mV dec^{-1}. The number of electrons transferred per oxygen molecule (*n*) was calculated to be 1.74, indicating a two-electron transfer process (Fig. S3a). In contrast, the NiO-Al-Co/carbon cloth exhibited a limiting current density of −6.20 mA cm^{-2} at 0.4 V (vs. RHE) with a Tafel slope of 248.5 mV dec^{-1}, showing the improved ORR activity. However, the number of electrons transferred was determined to be 1.79 (Fig. S3b), indicating that the two-electro transfer process did not change through the co-doping of Al and Co. In the OER region, the NiO/carbon cloth and NiO-Al-Co/carbon cloth delivered 10 mA cm^{-2} at the potentials of 1.547 and 1.530 V (vs. RHE), respectively, and the Tafel slopes were 71.7 and 77.3 mV dec^{-1}, respectively. Thus, the OER activity of the NiO-Al-Co/carbon cloth was also improved. The increased ORR and OER activity may be caused by the element doping, since Co was reported to have good activity toward oxygen electrocatalysis in alkaline solutions [39,40], while the detailed mechanisms in the doping states need further investigations. The stability of the NiO-Al-Co/carbon cloth toward the ORR and OER was further evaluated. As shown in Figs. 4c and 4d, after operating for 20 h, 80% of the initial current density was preserved for the ORR process, and the potential to achieve the current density of 10 mA cm^{-2} only increased 0.018 V for the OER process, illustrating the high stability during the electrocatalytic processes.

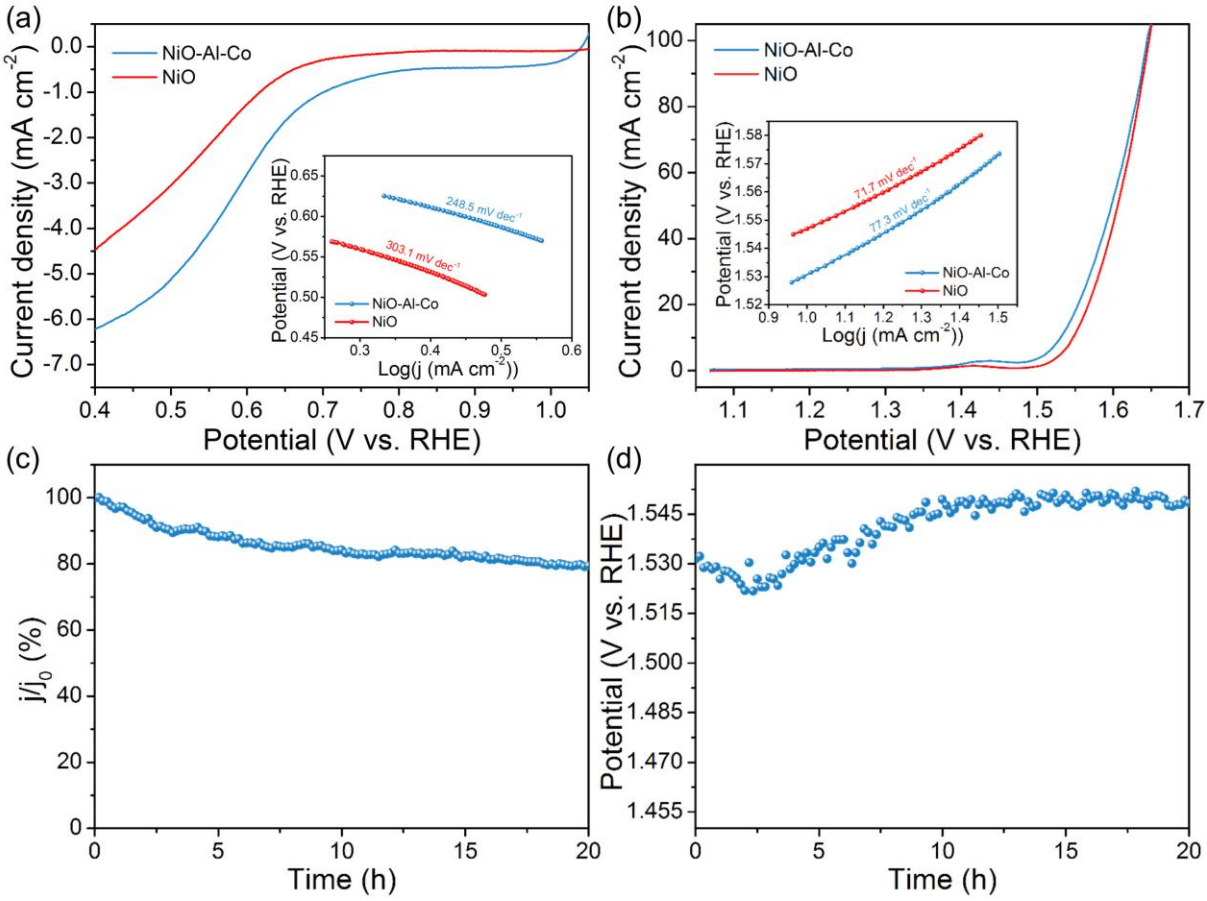

Fig. 4 Electrochemical activities of NiO and NiO-Al-Co nanosheets decorated carbon cloth for oxygen reactions in 0.1 M KOH electrolyte. (a-b) LSV curves of (a) ORR and (b) OER at a scan rate of 5 mV s^{-1}, the inset shows the corresponding Tafel plots. (c) ORR chronoamperometric response of NiO-Al-Co nanosheets decorated carbon cloth at a constant potential of 0.40 V (vs. RHE). (d) OER chronopotentiometric response of NiO-Al-Co nanosheets decorated carbon cloth at a constant current density of 10 mA cm^{-2}.

It is noticed that a small peak appears prior to the OER process (Fig. 4b). To further investigate the redox behavior of NiO and NiO-Al-Co nanosheets, the CV measurements were performed in the potential range of 1.066 to 1.566 V (vs. RHE) at various scan rates. As shown in Fig. S4, the non-rectangular shapes reveal the reversible redox reactions between Ni^{2+} and Ni^{3+} [41]. With the scan rate increases, the anodic and cathodic peaks shifted toward the positive and negative potentials, respectively, and the current density increased

accordingly, indicating the good rate performance (Figs. S4a and S4b). It is interesting to find that the CV shapes of both electrodes are similar, while the current density of NiO-Al-Co nanosheets is higher that of NiO nanosheets (Figs. S4c), and the corresponding capacitance also increases. Previous research indicated that Co doping can suppress the oxidation of Ni^{2+} to a higher oxidation state and lead to a slightly decreased capacity [24], while Al doping can increase the capacity due to an increased electrochemical surface area resulting from the morphology change [23]. As a result, the Al and Co co-doped NiO nanosheets lead to an increased pseudocapacitance, which is beneficial for the performance of batteries with this NiO-Al-Co/carbon cloth electrode.

3.3 Performance in Zn-air batteries

Before testing the electrochemical performance of NiO and NiO-Al-Co nanosheets decorated carbon cloth in Zn-air batteries, a polytetrafluoroethylene (PTFE) coating process was applied on the electrode to establish triple-phase boundaries that facilitate the gaseous oxygen transport [42]. The discharge and charge polarization curves are shown in Fig. 5a. For the initial discharge process, the battery with the NiO-Al-Co/carbon cloth electrode delivered a peak power density of 36.3 mW cm^{-2} at 71 mA cm^{-2}. Compared with some reported power densities of the electrodes made by the combination of the catalyst, carbon additives, and polymer binders [6], this low power may be caused by the poor conductivity due to the absence of carbon and high transport resistance [43], since an integrated electrode made of highly-active Co_3O_4 nanowire array was reported to deliver a maximum power density of only ~40 mW cm^{-2} [44]. During charge, interestingly, two voltage regions can be clearly observed. The first region near 1.9 V is related to the oxidation of nickel species [22], while the second one corresponds to the OER process, and the voltage increases to 2.5 V when the current density researches a high value of 116 mA cm^{-2}. This good charge performance may come from the hierarchical porous structure of the assembled nanosheets, which favors the

rapid charge transfer and facilitates the release of produced oxygen. Consequently, in the following discharge polarization curve as shown in Fig. S5, two distinct voltage regions were presented where the higher one above 1.5 V is related to the reduction of nickel species, and the lower one corresponds to the ORR. Thus, the Zn-air battery with the NiO-Al-Co/carbon cloth electrode exhibited the combined behaviors of Zn-Ni and Zn-air batteries and worked as a hybrid battery as reported [22,42,45,46]. To further demonstrate the hybrid properties, the battery was cycled at 5 mA cm^{-2}. As shown in Fig. 5b, in the first discharge stage, the flat voltage plateau at 1.14 V illustrated the ORR process occurs in a typical zinc-air battery. While in the charge stage, different from its single voltage profile, two voltage regions were presented, which correspond to the oxidation of Ni^{2+} to Ni^{3+} before 1.9 V and the OER afterward. In the following discharge stage, the reduction of Ni^{3+} to Ni^{2+} occurred first and resulted in a high voltage region, followed by the ORR and the resultant voltage plateau. Due to the limited pseudocapacitance (Fig. S4), the Zn-Ni reaction region is not so obvious in the present test. For rechargeable metal-air batteries, a fixed capacity is generally used for charge-discharge cycles to avoid the failure of reaction boundaries [4,47–49]. Hence, it can be deduced that in a limited cycling capacity, the contribution from Zn-Ni reaction can be large in the hybrid behaviors [45]. The increased discharge voltage and the decreased charge voltage owing to the redox reactions will lead to improved energy efficiency [45,46].

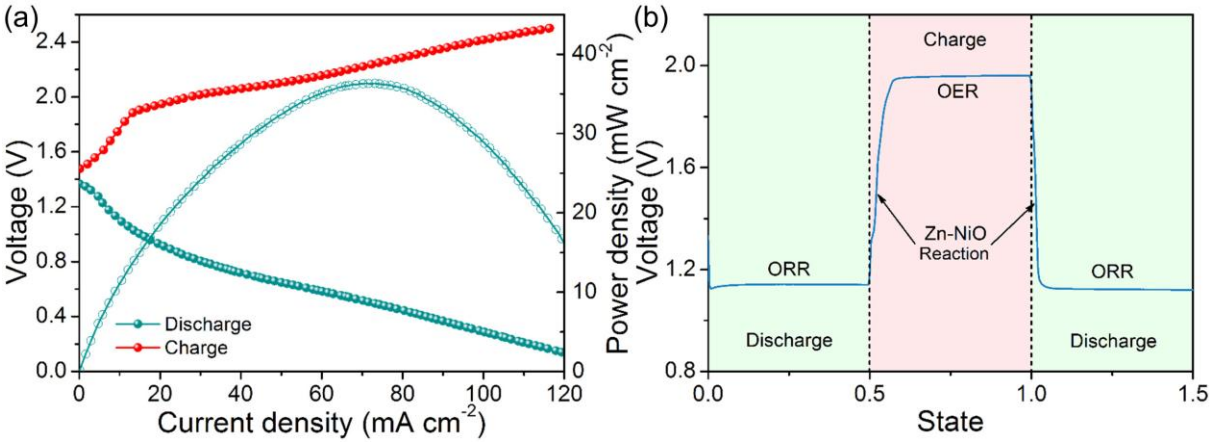

Fig. 5 Electrochemical performance of the Zn-air battery with the NiO-Al-Co/carbon cloth electrode. (a) Polarization curves and the corresponding power density. (b) Discharge-charge-discharge voltage profiles at current densities of 5 mA cm^{-2}.

The cycling stability of Zn-air batteries with the NiO and NiO-Al-Co nanosheets decorated carbon cloth was examined by pulse discharge-charge tests at 5 mA cm^{-2}, and compared with the one using the commercial catalysts of Pt/C and Ir/C. For the battery with NiO/carbon cloth, as shown in Fig. S6, a lower discharge voltage, higher charge voltage, and lower capacity from Zn-Ni reaction were presented when compared with the battery with NiO-Al-Co/carbon cloth electrode, consistent with the electrochemical performance in 0.1 M KOH (Figs. 4 and S4). Even so, stable discharge and charge voltages in the range of 1.03 and 1.96 V were maintained for 350 cycles, and the energy efficiency was higher than 57%. For the NiO-Al-Co/carbon cloth electrode, as shown in Fig. 6, the battery delivered a discharge voltage of 1.14 V and a charge voltage of 1.95 V in the first cycle. In comparison, the battery with the electrode made of Pt/C and Ir/C initially delivered the discharge and charge voltages of 1.24 V and 1.97 V, respectively. The higher discharge voltage may come from Pt/C as an effective catalyst for the ORR, however, the charge voltage was higher than that of NiO-Al-Co nanosheets even using the effective catalyst of Ir/C for the OER. This may be attributed to the electrode structure in which small pores are formed by carbon particles (Fig. S8), increasing the resistance of electrolyte accessibility and hindering the fast release of gaseous oxygen during the OER process [50]. In contrast, NiO-Al-Co nanosheets are in-situ grown on the carbon fiber surface to form a hierarchical porous structure. The mesopores are favorable for the rapid charge transfer, while the macropores formed by the interconnected nanosheets facilitate the release of produced oxygen, which together result in a low charge voltage. With an increase in the cycle number, for the battery using Pt/C and Ir/C, the discharge voltage gradually decreased, and the charge voltage increased, which may be caused by carbon

corrosion [51,52]. Eventually, the battery failed at the 401st cycle. For the battery using the NiO-Al-Co/carbon cloth electrode, even after 1000 cycles (333 h), the voltage gap changed from 815.9 mV to 881.7 mV (Fig. 6 insets), with an increase of only 65.8 mV, demonstrating the excellent stability. When looking inside of the cycling results of the NiO-Al-Co/carbon cloth electrode, as shown in Fig. S9a, the two-step voltage profile was retained throughout the cycling test. The capacity of the Zn-Ni reaction over the first 370 cycles gradually increased, which may be caused by the increase of the electroactive sites accessible by the electrolyte [42,46]. Then, the capacity showed a little decrease and became stable after 600 cycles (Fig. S9b). In a reported Zn-NiO battery, the capacity retention was 65% after 500 cycles. Hence, the co-doping of Al and Co successfully increased the stability of NiO in the redox reaction [24]. The energy efficiency during cycling was maintained to be around 62%, higher than that obtained from NiO nanosheets (Fig. S9c). After 1000 cycles, we also examined the electrode to observe the changes. As the SEM images and the XRD pattern shown in Fig. S10, both nanosheet morphology and the NiO phase were well maintained, confirming the stability after the long-term cycling test. It is worth noting that in present work, we focused on the air electrode applied in Zn-air batteries. For practical applications, the accumulation of carbon dioxide and the evaporation of water affect the ionic conductivity of the electrolyte [53], lowering the electrochemical performance during cycling. In addition, the formation and growth of dendrite in the Zn electrode can cause short-circuits and threaten the safety [6]. Therefore, the future research topics should be extended to stabilizing the electrolyte and suppressing the dendrite formation for the stable operation [54].

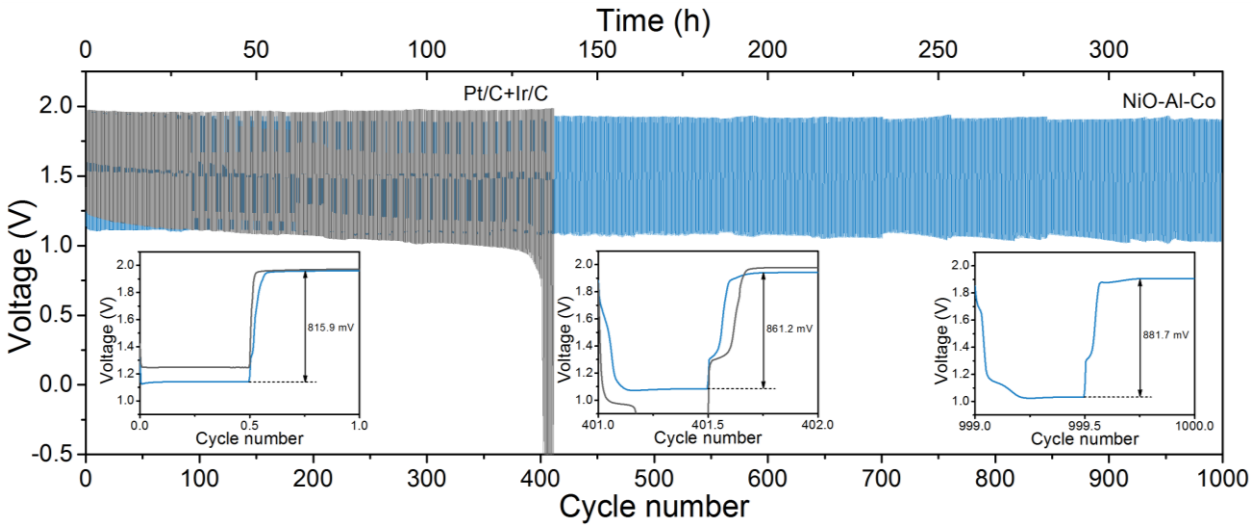

Fig. 6 Long-term cycling stability of Zn-air batteries with the NiO-Al-Co/carbon cloth and Pt/C+Ir/C electrode at 5 mA cm^{-2}, each cycle consists of 10 min discharge followed by 10 min charge. The insets show the voltage profiles of selected cycles.

4. Conclusions

In this work, we have developed an electrode made of Al and Co co-doped NiO nanosheets on carbon cloth. The SEM and TEM images show that porous nanosheets are directly grown on the surface of carbon fibers without the addition of binders, facilitating the transport of electrons. Additionally, the hierarchical structure shortens the length for species transport and provides abundant active sites for reactions. The EDS and XPS analyses indicate that the successful incorporation of Al and Co into NiO, which is unique for stabilizing the phase. In the alkaline solution, the Al and Co co-doped NiO electrode exhibits higher activity in both ORR and OER and superior stability than the pristine NiO electrode without doping. When assembled in a Zn-air battery, the NiO-Al-Co/carbon cloth electrode exhibits a peak power density of 36.3 mW cm^{-2}. Moreover, combined behaviors from Zn-Ni and Zn-air batteries are presented, which come from the redox reactions of NiO. When cycling the battery with the Al and Co co-doped NiO nanosheets electrode at 5 mA cm^{-2}, impressively, stable voltage gaps of ~0.82 V and energy efficiency of 62% over 1000 cycles

(330 h) are exhibited. In comparison, a battery with the electrode made of Pt/C and Ir/C shows increasing voltage gaps and can only be operated for 400 cycles. The characterization of the electrode after cycling illustrates that both the nanosheet morphology and the NiO phase are well maintained. Hence, the Al and Co co-doped NiO nanosheets on carbon cloth is a promising air electrode to enable the high cycling stability of rechargeable Zn-air batteries.

Acknowledgments

M. Ni thanks the funding support from The Hong Kong Polytechnic University (G-YW2D) and a grant (Project Number: PolyU 152214/17E) from Research Grant Council, University Grants Committee, Hong Kong SAR.

References

[1] Z.P. Cano, D. Banham, S. Ye, A. Hintennach, J. Lu, M. Fowler, Z. Chen, Batteries and fuel cells for emerging electric vehicle markets, Nat. Energy. 3 (2018) 279–289.

[2] P. Tan, H.R. Jiang, X.B. Zhu, L. An, C.Y. Jung, M.C. Wu, L. Shi, W. Shyy, T.S. Zhao, Advances and challenges in lithium-air batteries, Appl. Energy. 204 (2017) 780–806.

[3] M.A. Rahman, X. Wang, C. Wen, High Energy Density Metal-Air Batteries: A Review, J. Electrochem. Soc. 160 (2013) A1759–A1771.

[4] Y. Li, J. Lu, Metal–Air Batteries: Will They Be the Future Electrochemical Energy Storage Device of Choice?, ACS Energy Lett. 2 (2017) 1370–1377.

[5] R. Schmuch, R. Wagner, G. Hörpel, T. Placke, M. Winter, Performance and cost of materials for lithium-based rechargeable automotive batteries, Nat. Energy. 3 (2018) 267–278.

[6] J. Fu, Z.P. Cano, M.G. Park, A. Yu, M. Fowler, Z. Chen, Electrically Rechargeable Zinc-Air Batteries: Progress, Challenges, and Perspectives, Adv. Mater. 29 (2017) 1604685.

[7] E. Hu, X. Yang, Rejuvenating zinc batteries, Nat. Mater. 17 (2018) 480–481.

[8] Y. Li, H. Dai, Recent advances in zinc–air batteries, Chem. Soc. Rev. 43 (2014) 5257–5275.

[9] J.-I. Jung, M. Risch, S. Park, M.G. Kim, G. Nam, H.-Y. Jeong, Y. Shao-Horn, J. Cho, Optimizing nanoparticle perovskite for bifunctional oxygen electrocatalysis-ESI, Energy Environ. Sci. 9 (2016) 176–183.

[10] K.-N. Jung, J. Kim, Y. Yamauchi, M.-S. Park, J.-W. Lee, J.H. Kim, Rechargeable lithium–air batteries: a perspective on the development of oxygen electrodes, J. Mater. Chem. A. 4 (2016) 14050–14068.

[11] P. Tan, M. Liu, Z. Shao, M. Ni, Recent Advances in Perovskite Oxides as Electrode Materials for Nonaqueous Lithium-Oxygen Batteries, Adv. Energy Mater. 7 (2017) 1602674.

[12] Z.-F. Huang, J. Wang, Y. Peng, C.-Y. Jung, A. Fisher, X. Wang, Design of Efficient Bifunctional Oxygen Reduction/Evolution Electrocatalyst: Recent Advances and Perspectives, Adv. Energy Mater. 7 (2017) 1700544.

[13] S. Liu, I.S. Amiinu, X. Liu, J. Zhang, M. Bao, T. Meng, S. Mu, Carbon nanotubes intercalated Co/N-doped porous carbon nanosheets as efficient electrocatalyst for oxygen reduction reaction and zinc–air batteries, Chem. Eng. J. 342 (2018) 163–170.

[14] L.-A. Stern, X. Hu, Enhanced oxygen evolution activity by NiO_x and $Ni(OH)_2$ nanoparticles, Faraday Discuss. 176 (2014) 363–379.

[15] D. Chen, C. Chen, Z.M. Baiyee, Z. Shao, F. Ciucci, Nonstoichiometric Oxides as Low-Cost and Highly-Efficient Oxygen Reduction/Evolution Catalysts for Low-Temperature Electrochemical Devices, Chem. Rev. 115 (2015) 9869–9921.

[16] M. Chhetri, S. Sultan, C.N.R. Rao, Electrocatalytic hydrogen evolution reaction activity comparable to platinum exhibited by the $Ni/Ni(OH)_2$/graphite electrode, Proc. Natl. Acad. Sci. (2017) 201710443.

[17] G. Li, M.A. Mezaal, K. Zhang, L. Lei, Synthesis and Electrocatalytic Performance of NiO Modified Co_3O_4 Composites for Zinc-Air Batteries, Int. J. Electrochem. Sci. 10 (2015) 5395–5404.

[18] B. Li, S.-W. Chien, X. Ge, J. Chai, X.-Y. Goh, K.-T. Nai, T.S. Andy Hor, Z. Liu, Y. Zong, Ni/NiO_x -decorated carbon nanofibers with enhanced oxygen evolution activity for rechargeable zinc–air batteries, Mater. Chem. Front. 1 (2017) 677–682.

[19] J. Yin, Y. Li, F. Lv, Q. Fan, Y.-Q. Zhao, Q. Zhang, W. Wang, F. Cheng, P. Xi, S. Guo, NiO/CoN Porous Nanowires as Efficient Bifunctional Catalysts for Zn–Air Batteries, ACS Nano. 11 (2017) 2275–2283.

[20] J. Fang, L. Hu, M. Wang, L. Gan, C. Chen, Y. Jiang, B. Xiao, Y. Lai, J. Li, NiO-Fe2O3/carbon nanotubes composite as bifunctional electrocatalyst for rechargeable Zn-air batteries, Mater. Lett. 218 (2018) 36–39.

[21] P. Tan, B. Chen, H. Xu, W. Cai, M. Liu, Z. Shao, M. Ni, Nanoporous NiO/$Ni(OH)_2$ Plates Incorporated with Carbon Nanotubes as Active Materials of Rechargeable Hybrid Zinc Batteries for Improved Energy Efficiency and High-Rate Capability, J. Electrochem. Soc. 165 (2018) A2119–A2126.

[22] D.U. Lee, J. Fu, M.G. Park, H. Liu, A. Ghorbani Kashkooli, Z. Chen, Self-Assembled NiO/$Ni(OH)_2$ Nanoflakes as Active Material for High-Power and High-Energy Hybrid Rechargeable Battery, Nano Lett. 16 (2016) 1794–1802.

[23] H. Wang, Z. Tang, Y. Liu, C. Lee, Synthesis and behavior of Al-stabilized α-Ni(OH)2, Trans. Nonferrous Met. Soc. China. 19 (2009) 170–175.

[24] Y.L. Zhao, J.M. Wang, H. Chen, T. Pan, J.Q. Zhang, C.N. Cao, Different additives-substituted α-nickel hydroxide prepared by urea decomposition, Electrochim. Acta. 50 (2004) 91–98.

[25] X. Kong, J. Zhao, W. Shi, Y. Zhao, M. Shao, M. Wei, L. Wang, X. Duan, Fabrication

of aluminum-doped α-Ni(OH)2 with hierarchical architecture and its largely enhanced electrocatalytic performance, Electrochim. Acta. 80 (2012) 257–263.

[26] R.S. Jayashree, P. Vishnu Kamath, Layered double hydroxides of Ni with Cr and Mn as candidate electrode materials for alkaline secondary cells, J. Power Sources. 107 (2002) 120–124.

[27] L. Xie, Z. Hu, C. Lv, G. Sun, J. Wang, Y. Li, H. He, J. Weng, K. Li, Co xNi 1-x double hydroxide nanoparticles with ultrahigh specific capacitances as supercapacitor electrode materials, Electrochim. Acta. 78 (2012) 205–211.

[28] M. Gong, Y. Li, H. Zhang, B. Zhang, W. Zhou, J. Feng, H. Wang, Y. Liang, Z. Fan, J. Liu, H. Dai, Ultrafast high-capacity NiZn battery with NiAlCo-layered double hydroxide, Energy Environ. Sci. 7 (2014) 2025–2032.

[29] H. Long, T. Shi, H. Hu, S. Jiang, S. Xi, Z. Tang, Growth of Hierarchal Mesoporous NiO Nanosheets on Carbon Cloth as Binder-free Anodes for High-performance Flexible Lithium-ion Batteries, Sci. Rep. 4 (2015) 7413.

[30] R.R. Salunkhe, J. Lin, V. Malgras, S.X. Dou, J.H. Kim, Y. Yamauchi, Large-scale synthesis of coaxial carbon nanotube/$Ni(OH)_2$ composites for asymmetric supercapacitor application, Nano Energy. 11 (2015) 211–218.

[31] P. Tan, B. Chen, H. Xu, W. Cai, W. He, M. Ni, Investigation on the electrode design of hybrid Zn-Co3O4 /air batteries for performance improvements, Electrochim. Acta. 283 (2018) 1028-1036.

[32] M. Gong, Y. Li, H. Zhang, B. Zhang, W. Zhou, J. Feng, H. Wang, Y. Liang, Z. Fan, J. Liu, H. Dai, Ultrafast high-capacity NiZn battery with NiAlCo-layered double hydroxide, Energy Environ. Sci. 7 (2014) 2025.

[33] F. Cheng, J. Chen, Lithium-air batteries: Something from nothing, Nat. Chem. 4 (2012) 962–963.

[34] Z. Zhu, J. Ping, X. Huang, J. Hu, Q. Chen, X. Ji, C.E. Banks, Hexagonal nickel oxide nanoplate-based electrochemical supercapacitor, J. Mater. Sci. 47 (2012) 503–507.

[35] X. Xiong, G. Waller, D. Ding, D. Chen, B. Rainwater, B. Zhao, Z. Wang, M. Liu, Controlled synthesis of $NiCo_2S_4$ nanostructured arrays on carbon fiber paper for high-performance pseudocapacitors, Nano Energy. 16 (2015) 71–80.

[36] Q. Zhang, B. Zhao, J. Wang, C. Qu, H. Sun, K. Zhang, M. Liu, High-performance hybrid supercapacitors based on self-supported 3D ultrathin porous quaternary Zn-Ni-Al-Co oxide nanosheets, Nano Energy. 28 (2016) 475–485.

[37] Y. Sun, J. Liu, J. Song, S. Huang, N. Yang, J. Zhang, Y. Sun, Y. Zhu, Exploring the Effect of Co3O4 Nanocatalysts with Different Dimensional Architectures on Methane Combustion, ChemCatChem. 8 (2016) 540–545.

[38] W. Luo, X. Hu, Y. Sun, Y. Huang, Electrospun porous $ZnCo_2O_4$ nanotubes as a high-performance anode material for lithium-ion batteries, J. Mater. Chem. 22 (2012) 8916–8921.

[39] Y. Li, M. Gong, Y. Liang, J. Feng, J.E. Kim, H. Wang, G. Hong, B. Zhang, H. Dai, Advanced zinc-air batteries based on high-performance hybrid electrocatalysts, Nat Commun. 4 (2013) 1805.

[40] V. Caramia, B. Bozzini, Materials science aspects of zinc–air batteries: a review, Mater. Renew. Sustain. Energy. 3 (2014) 28.

[41] Y.P. Wu, X. Wang, M. Li, Y. Wang, B. Chen, Y. Zhu, A Zn-NiO rechargeable battery with long lifespan and high energy density, J. Mater. Chem. A. 3 (2015) 8280–8283.

[42] B. Li, J. Quan, A. Loh, J. Chai, Y. Chen, C. Tan, X. Ge, T.S.A. Hor, Z. Liu, H. Zhang, Y. Zong, A robust hybrid zn-battery with ultralong cycle life, Nano Lett. 17 (2017) 156–163.

[43] F. Cheng, J. Chen, Metal–air batteries: from oxygen reduction electrochemistry to

cathode catalysts, Chem. Soc. Rev. 41 (2012) 2172–2192.

[44] D.U. Lee, J.-Y. Choi, K. Feng, H.W. Park, Z. Chen, Advanced Extremely Durable 3D Bifunctional Air Electrodes for Rechargeable Zinc-Air Batteries, Adv. Energy Mater. 4 (2014) 1301389.

[45] A. Qaseem, F. Chen, C. Qiu, A. Mahmoudi, X. Wu, X. Wang, R.L. Johnston, Reduced Graphene Oxide decorated with Manganese Cobalt Oxide as Multifunctional Material for Mechanically Rechargeable and Hybrid Zinc-Air Batteries, Part. Part. Syst. Charact. 34 (2017) 1700097.

[46] P. Tan, B. Chen, H. Xu, W. Cai, W. He, M. Liu, Z. Shao, M. Ni, Co_3O_4 Nanosheets as Active Material for Hybrid Zn Batteries, Small. 14 (2018) 1800225.

[47] J. Lu, L. Li, J.B. Park, Y.K. Sun, F. Wu, K. Amine, Aprotic and aqueous Li-O_2 batteries, Chem. Rev. 114 (2014) 5611–5640.

[48] M. Lu, C. Xu, Y. Zhan, J.Y. Lee, Improving the Performance of Perovskite in Nonaqueous Oxygen Electrocatalysis, Chem. - An Asian J. 11 (2016) 1210–1217.

[49] P. Tan, W. Shyy, M.C. Wu, Y.Y. Huang, T.S. Zhao, Carbon electrode with NiO and RuO_2 nanoparticles improves the cycling life of non-aqueous lithium-oxygen batteries, J. Power Sources. 326 (2016) 303–312.

[50] P. Tan, W. Shyy, Z.H. Wei, L. An, T.S. Zhao, A carbon powder-nanotube composite cathode for non-aqueous lithium-air batteries, Electrochim. Acta. 147 (2014) 1–8.

[51] J.W.D. Ng, M. Tang, T.F. Jaramillo, A carbon-free, precious-metal-free, high-performance O_2 electrode for regenerative fuel cells and metal–air batteries, Energy Environ. Sci. 7 (2014) 2017.

[52] C. Ma, N. Xu, J. Qiao, S. Jian, J. Zhang, Facile synthesis of NiCo2O4 nanosphere-carbon nanotubes hybrid as an efficient bifunctional electrocatalyst for rechargeable Zn–air batteries, Int. J. Hydrogen Energy. 41 (2016) 9211–9218.

[53] J.-S. Lee, S.T. Kim, R. Cao, N.-S. Choi, M. Liu, K.T. Lee, J. Cho, Metal-Air Batteries with High Energy Density: Li-Air versus Zn-Air, Adv. Energy Mater. 1 (2011) 34–50.

[54] P. Tan, B. Chen, H. Xu, H. Zhang, W. Cai, M. Ni, M. Liu, Z. Shao, Flexible Zn– and Li–air batteries: recent advances, challenges, and future perspectives, Energy Environ. Sci. 10 (2017) 2056–2080.